ICES Journal of Marine Science Advance Access published April 14, 2015

ICES Journal of Marine Science

ICES International Council for the Exploration of the Sea
CIEM Conseil International pour l'Exploration de la Mer

ICES Journal of Marine Science; doi:10.1093/icesjms/fsv062

Combining otolith microstructure and trace elemental analyses to infer the arrival of juvenile Pacific bluefin tuna in the California current ecosystem

Hannes Baumann[1]*, R. J. D. Wells[2,3], Jay R. Rooker[2,3], Saijin Zhang[2], Zofia Baumann[1], Daniel J. Madigan[4], Heidi Dewar[5], Owyn E. Snodgrass[6], and Nicholas S. Fisher[4]

[1]*Department of Marine Sciences, University of Connecticut, 1080 Shennecossett Road, Groton, CT 06340-6048, USA*
[2]*Department of Marine Biology, Texas A&M University, 1001 Texas Clipper Road, Galveston, TX 77553, USA*
[3]*Department of Wildlife and Fisheries Sciences, Texas A&M University, College Station, Texas, TX 77843, USA*
[4]*School of Marine and Atmospheric Sciences, Stony Brook University, Dana Hall, Stony Brook, NY 11794-5000, USA*
[5]*Fisheries Resources Division, Southwest Fisheries Science Center, National Marine Fisheries Service, NOAA, 8901 La Jolla Shores Drive, La Jolla, CA 92037, USA*
[6]*Ocean Associates, Incorporated, Southwest Fisheries Science Center, National Marine Fisheries Service, NOAA, 8901 La Jolla Shores Drive, USA, La Jolla, CA 92037, USA*

**Corresponding author: tel: +1 860 405 9297; e-mail: hannes.baumann@uconn.edu*

Baumann, H., Wells, R. J. D., Rooker, J. R., Zhang, S., Baumann, Z., Madigan, D. J., Dewar, H., Snodgrass, O. E., and Fisher, N. S. Combining otolith microstructure and trace elemental analyses to infer the arrival of juvenile Pacific bluefin tuna in the California current ecosystem. – ICES Journal of Marine Science, doi: 10.1093/icesjms/fsv062.

Received 7 January 2015; revised 16 March 2015; accepted 19 March 2015.

Juvenile Pacific bluefin tuna (PBT, *Thunnus orientalis*) are known to migrate from western Pacific spawning grounds to their eastern Pacific nursery and feeding grounds in the California Current Large Marine Ecosystem (CCLME), but the timing, durations, and fraction of the population that makes these migrations need to be better understood for improved management. To complement recent work focused on stable isotope and radiotracer approaches ("tracer toolbox"; Madigan *et al.*, 2014) we explored the suitability of combining longitudinal analyses of otolith microstructure and trace elemental composition in age ~1–2 PBT ($n = 24$, 66–76 cm curved fork length) for inferring the arrival of individuals in the CCLME. Element:Ca ratios in transverse otolith sections (9–12 rows, triplicate ablations from primordium to edge, ø50 μm) were quantified for eight elements: Li, Mg, Mn, Co, Cu, Zn, Sr, and Ba, which was followed by microstructure analysis to provide age estimates corresponding to each ablation spot. Age estimates from otoliths ranged from 328 to 498 d post-hatch. The combined elemental signatures of four elements (Ba, Mg, Co, Cu) showed a significant increase at the otolith edge in approximately half of the individuals (30–60 d before catch). Given the different oceanographic properties of oligotrophic open Pacific vs. high nutrient, upwelling CCLME waters, this signal is consistent with the entry of the fish into the CCLME, which was estimated to occur primarily in July after a transoceanic migration of ~1.5–2.0 months. Our approach comprises a useful addition to the available tracer toolbox and can provide additional and complementary understanding of trans-Pacific migration patterns in PBT.

Keywords: barium, LA-ICPMS, magnesium, migration, *Thunnus orientalis*.

Introduction

Pelagic predators such as tunas and sharks often undertake large oceanic migrations at different stages of their life, which makes the sustainable management of these species a complex and formidable challenge (Rooker *et al.*, 2008; Block *et al.*, 2011). Bluefin tuna (*Thunnus thynnus*, *T. orientalis*, *and T. maccoyii*) are known to migrate across entire ocean basins (Collette and Nauen, 1983; Bayliff, 1994; Rooker *et al.*, 2007), and their long lifespan

and high market value contribute to their vulnerability to overfishing and population collapse (Collette *et al.*, 2011). The Pacific bluefin tuna (PBT, *T. orientalis*), one of the most highly priced fish on the market and currently depleted to <6% of its presumed pre-fished population levels (ISC, 2014), is an iconic example of this predicament. PBT spawn in late spring to summer in the western Pacific Ocean (Kitagawa *et al.*, 1995; Chen *et al.*, 2006; Suzuki *et al.*, 2014), and an unknown fraction of the juveniles migrate across the North Pacific Ocean during their first or second year of life to reach the California Current Large Marine Ecosystem (CCLME), one of the world's major upwelling regions and a favourable tuna feeding ground (Bayliff, 1994; Block *et al.*, 2011). Most PBT spend several years in the CCLME before undertaking the trans-Pacific return journey to their spawning grounds as mature adults (Bayliff *et al.*, 1991; Boustany *et al.*, 2010).

To improve management, several studies have recently investigated juvenile PBT migration and residency patterns in the CCLME, specifically by using chemical tracers (Madigan *et al.*, 2012, 2013, 2014). Madigan *et al.* (2014) developed a "tracer toolbox" consisting of stable isotope analyses (i.e. bulk $\delta^{15}N$ and amino acid compound-specific isotope analysis, AA-CSIA) and measurements of anthropogenic radiocesium (^{134}Cs and ^{137}Cs) that was released into the western Pacific Ocean off Japan following the Fukushima nuclear accident in spring 2011 (Buesseler *et al.*, 2012). The premise behind stable isotope and radiocesium "clocks" is that exposure differs between waters of the western and eastern Pacific Ocean, i.e. between relatively $\delta^{15}N$ depleted, oligotrophic waters with elevated Cs levels (expected initial ^{134}Cs:^{137}Cs ratio =1, Buesseler *et al.*, 2012) and $\delta^{15}N$ enriched, upwelling waters of the CCLME with no ^{134}Cs and low ^{137}Cs (expected ^{134}Cs:^{137}Cs ratio =0), respectively (Madigan *et al.*, 2014). If the movement of fish between these different ocean regions results in measurable changes of these tracers in their muscle tissue, they can be used retrospectively to infer past migration and residency patterns.

Here we test the suitability of adding a third tool to the "tracer toolbox", using otoliths instead of muscle tissue samples to infer PBT migration patterns. Calcified fish otoliths are arguably the most widely used animal hard structure in biological oceanography (Campana, 2005), because they are continuously formed during a fish's life (but never re-formed) and because the rate and biochemical composition of otolith protein + $CaCO_3$ accretion varies relative to abiotic factors (e.g. temperature and elemental composition of seawater) and biotic factors (e.g. somatic growth and ontogenetic stage). Hence, otoliths offer the reconstruction of a suite of valuable oceanographic and biological information. Otolith macrostucture analyses have generally focused on inferring yearly age and growth for stock assessment purposes (Campana, 2001) or biochronologies (Morrongiello *et al.*, 2012). Otolith microstructure analyses interpret daily growth structures during the larval and juvenile stages to infer hatch time, age, growth, or selective mortality (e.g. Stevenson and Campana, 1992; Baumann *et al.*, 2006). Otolith microchemistry, on the other hand, attempts to reconstruct the movement of fish through specific water bodies, based on measuring concentrations of stable isotopes such as $\delta^{13}C$ or $\delta^{18}O$ (Thorrold *et al.*, 1997) or various trace elements (Campana and Thorrold, 2001; Elsdon *et al.*, 2008). While most reliably used for inferring ontogenetic habitat changes in diadromous fish (Veinott and Porter, 2005; Kerr *et al.*, 2009), otolith elemental compositions have also been used with success to discriminate relative importance of different spawning grounds (e.g. cod: Campana *et al.*, 2000; PBT: Rooker *et al.*, 2001b), to reconstruct thermal habitat and feeding histories (Thorrold *et al.*, 1997), or to infer fish exposure to upwelling based on increased otolith Ba signatures (Woodson *et al.*, 2013).

This study hypothesized that juvenile PBT entering the CCLME experience a change from exposure to oligotrophic open Pacific to coastal upwelling waters, with the different geochemical properties potentially recorded and thus detectable in their otoliths. We chose a trace elemental approach and used Laser Ablation Inductively Coupled Plasma Mass Spectrometry (LA-ICPMS) to measure concentrations of eight elements (Li, Mg, Mn, Co, Cu, Zn, Sr, and Ba) in transversal otolith sections from juvenile PBT caught in late summer within the CCLME. We then added ontogenetic context to microchemistry data by conducting subsequent otolith microstructure analyses, which allowed back-calculating the date and age corresponding to each ablation spot. We used a replicated, longitudinal ablation pattern and devised a method to examine and digitally overlay the otolith microstructure. Because we were primarily interested in the arrival of PBT juveniles, our analyses focused on approximately the last 5 months before capture of each fish and evaluated whether Ba and potentially other trace elements changed in a pattern consistent with an entry signal into the coastal upwelling waters of the CCLME.

Methods

Field sampling and otolith preparation

Specimens were collected dockside as part of NOAA's biological sampling programme for recreational tuna caught off the coast of San Diego, CA, USA. In 2012, sagittal otoliths were extracted from a total of 349 PBT heads that were also measured for operculum length (OL). OL was used to estimate curved fork length (CFL), i.e. the fork length of each fish as if measured along its curved body ($CFL = 32.94 \times e^{0.037 \times OL}$). From this subsample, we randomly selected 25 juveniles that were most likely recent age-1 year immigrants to the CCLME, based on their narrow size range (CFL: 66.3–76.0 cm) and catch date (4 August–25 September 2012). Extracted otoliths were cleaned, stored air-dry, and then embedded in clear epoxy resin (Stuers EpoFix), before transversal sectioning through the primordium (~0.5 mm thickness, low speed IsoMet®, Buehler®). Sections were then mounted on glass sides with thermoplastic (=reheatable) cement (ChrystalBond©) that allowed polishing sections from both sides to ~300 μm thickness using 0.3 μm MicroPolish Alumina Powder and 1200-600 grit silicone-carbide paper (Buehler®).

Trace elemental measurements

Longitudinal patterns in trace elemental composition were assessed in the ventro-distal portion of transversal otolith sections (Figure 1) using an ultraviolet NWR 213 Laser ablation unit with a quadrupole Thermo Scientific XSeries II ICPMS. LA-ICPMS was deemed advantageous over micro-milling, primarily because it required the least amount of otolith material and thus had the best temporal resolution. Depending on otolith size, 29–40 spots of 50 μm diameter were ablated using laser energy, repeat rates, and ablation times of 60%, 10 Hz, and 12 s, respectively (for other parameters, see Supplemental material, Table S1). National Institute of Standards and Technology (NIST) glass 614 was used as the standard to create calibration curves for each element of interest. We assumed calcium to be evenly distributed at a concentration of 38% across the whole otolith and thus used it as the internal standard to correct variations in ablation yield and counting efficiencies

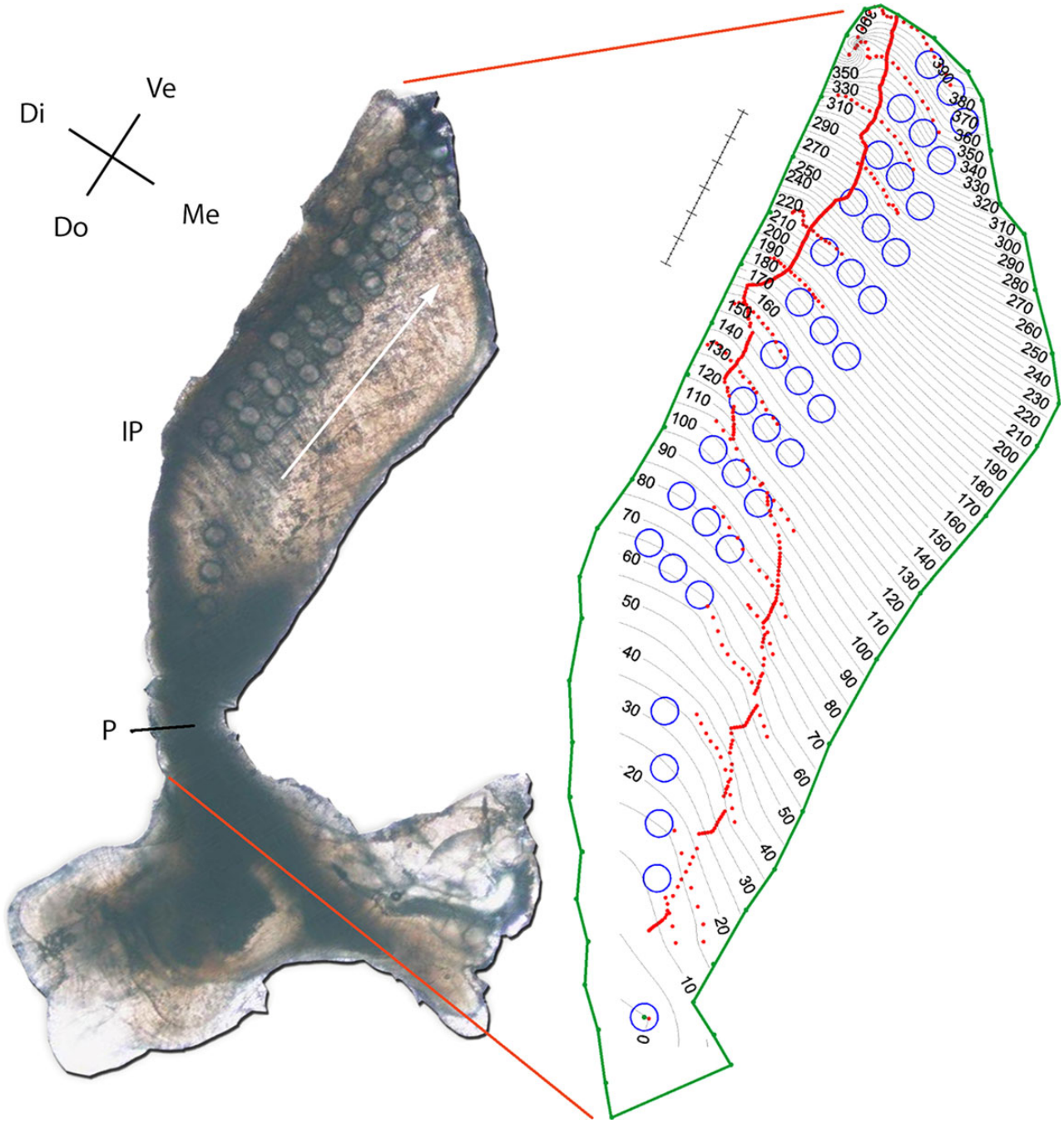

Figure 1. Transversal section of a juvenile PBT sagittal otolith after ablation (left, image) and its digitized representation after microstructure analysis (right, shape). Individual daily increments and age isolines (red dots) were marked across multiple images, combined, and used to construct an age grid (grey lines, contour labels = days) that allowed associating ages to each ablation crater. The approximate dorsal/ventral and distal/medial axes (black cross) are given for orientation, while the white arrow depicts the otolith growth axis. P, primordium, IP, inflection point. Scale bar for shape with major/minor ticks = 50/10 μm, respectively. This figure is available in black and white in print and in colour at *ICES Journal of Marine Science* online.

(Rooker *et al.*, 2001a). Trace element contamination was avoided by pre-ablating all targets and standards for 10 s before actual measurement ablations began. In addition, integration was applied only to the stable fragment of the spectrum (usually 5 s after ablation began), while air spectrum collected before each actual ablation was used as blank for correction. The first ablation spot was always set at the primordium (operationally defined as the narrowest part of the otolith section), followed by four equally spaced spots until the otolith inflection point (Figure 1). Thereafter, until the edge of the otolith, we used triplicate ablations in 8–12 rows of assumed same age, given that they were oriented perpendicularly to otolith growth axis (Figure 1). Concentrations were recorded for eight elements of interest: lithium (^{7}Li), magnesium (^{24}Mg), manganese (^{55}Mn), cobalt (^{59}Co), copper (^{65}Cu),

zinc (^{66}Zn), strontium (^{88}Sr), and barium (^{137}Ba). Elemental concentrations ([*E*], ppb) were then transformed into Element:Ca molar ratios (R_E, μmol mol^{-1}) based on the molar mass of each element (M_E, g mol^{-1}) and calcium (M_{Ca} =44 g mol^{-1}):

$$R_E = \frac{[E]}{1000}\left(M_E \frac{0.38}{M_{Ca}}\right)^{-1}.$$

Microstructure analysis

The same transversal otolith sections used for trace element measurements were subsequently used for microstructure analysis. To discern microstructural patterns, sections required further polishing from both sides to a final thickness of ~100 μm, which erased the ablation craters previously visible on the surface. Hence, before the post-ablation polish the section shape and the ablation spot positions were digitized (ImagePro 4.5) from a calibrated picture taken at low magnification (4×). After the final polish, sections were coated with a thin oil film that improved clarity, followed by taking calibrated digital pictures of up to 10 overlapping areas under ×400 magnification from the primordium to the edge. Each area was photographed 5–10 times under slightly different foci, which enhanced microstructure interpretability through merged multifocal images (.TIFF, ImagePro; see Baumann *et al.*, 2006). From the primordium to the otolith edge, presumed daily increments were opportunistically marked where they could be best discerned, which followed a similar but not a consistent axis (Figure 1) and precluded measurements of individual increment widths. All otoliths were read twice blind by the same reader (H.B.) and again a third time, if initial counts differed by more than 10% ($n = 8$). Assuming a learning curve, the second or third age reading was then chosen for further analysis. One specimen was excluded from further analysis due to poor image quality. The final mean coefficient of variation (CV_m) of age estimates across all 24 individuals was 5.7%, calculated according to Campana (2001) as

$$\mathrm{CV_m} = \frac{1}{24}\sum_{j=1}^{24} CV_j = 100\frac{\sqrt{\sum_{i=1}^{N}((X_{ij}-X_j)^2/\mathrm{N}-1)}}{X_j},$$

where X_{ij} is *i*th age reading of the *j*th individual with a mean age X_j and the number of readings *N*.

In addition to marking individual increments, we also digitized 15–20 age isolines per otolith by placing markers along specific increments that could be traced well (Figure 1). The coordinates of both age and age isoline markers were then transformed into coordinates relative to the otolith primordium and used to calculate an age contour grid (Kriging, Golden Software Surfer 8.0). The grid, the digitized otolith shape, and the ablation spots were then digitally overlaid (anchored by the primordium and outer shape as common landmarks), and minimum, mid, and maximum ages were manually extracted for each ablation spot (Figure 1). The temporal resolution of this approach decreased from primordium to edge, given that the days encompassed by each 50 μm ablation spot increased from ~5 d spot^{-1} near the primordium (widest increments) to 23–29 d spot^{-1} closest to the otolith edge (narrowest increments, Figure 2). Increments were generally unrecognizable within the first 100 μm from the primordium, which we assumed resulted in, and thus corrected for, an average underestimation of age by 30 d (Itoh *et al.*, 2000). The corrected, mid-age estimate of each ablation spot could then be used to describe average longitudinal patterns in R_E relative to day post-hatch (dph, e.g. Figure 4), day before catch (dpc, e.g. Figure 5), or the calendar date when the ablated material was likely deposited on the otolith (e.g. Figure 6). General trends in these measures were calculated across the replicate ablation points.

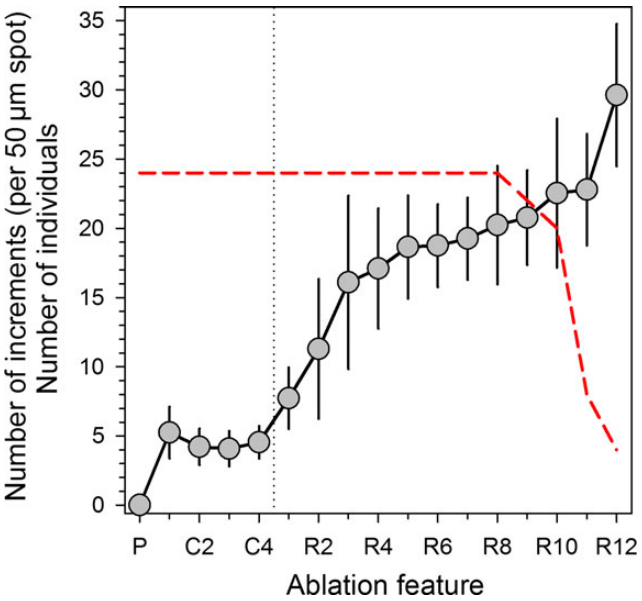

Figure 2. Average (± s.d.) number of micro-increments (d) estimated to be within each 50 μm ablation spot from the primordium to the edge of the otolith section. The dotted line separates single ablation spots between primordium (P) and the otolith inflection point (C1–C4) and rows of triplicate ablation spots (R1–R12). The red line shows the number of individuals for each ablation feature. Since marginal increments of each ablation spot contribute very little material, the actual age range is likely lower than the absolute age range shown here. This figure is available in black and white in print and in colour at *ICES Journal of Marine Science* online.

Results

The estimated age of PBT juveniles ranged from 328 to 498 dph (mean ± s.d.: 402 ± 41 d). Age was positively correlated with size (CFL, $p = 0.004$, $r^2 = 0.32$, Figure 3a) and sampling date ($r^2 = 0.43$, $p = 0.004$), whereas size and back-calculated hatch date were negatively correlated ($r^2 = 0.17$, $p = 0.044$). The hatch distribution ranged from April to September 2011, with a mode in July ($n = 9$, 38%) and a mean (s.d.) on 13 July 2011 (± 36 d). Twenty-one of 24 individuals (88%) hatched in June, July, and August 2011 (Figure 3b).

Average ontogenetic patterns in R_E were highly variable among elements (Figure 4a–h). R_{Li} and R_{Mg} showed a similar pattern of initially high values (2.9–6.8 and 210–580 μmol mol^{-1}, respectively) that declined rapidly over the first ~100 dph, followed by stable or slightly declining R_E values (1.4–3.3 and 110–230 μmol mol^{-1}, respectively; Figure 4a and b). R_{Mn} showed a remarkable longitudinal decline from high (2.8–7.9 μmol mol^{-1}) to low variability (0.5–1.7 μmol mol^{-1}) along with declining average values (Figure 4c). R_{Co} and R_{Cu} were mostly close to the detection limit (Supplementary material, Table S1) with the notable exception of some individuals that exhibited very high R_E values close to the primordium and again close to the

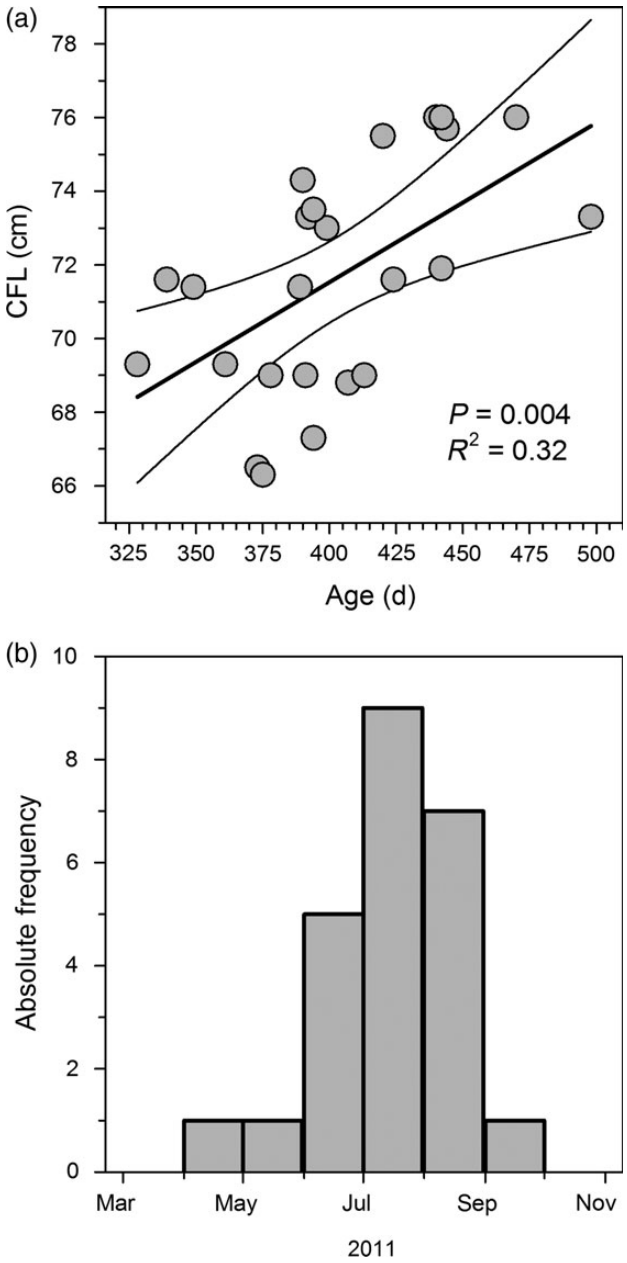

Figure 3. (a) Linear fit ($\pm$95% confidence intervals) to the relationship between-otolith inferred age (d, post-hatch) and CFL for the 24 juvenile PBT of this study; (b) Back-calculated hatch-date distribution in 2011 based on otolith-inferred age and sampling dates in 2012.

edge (up to 1.5 and 3.2 μmol mol^{-1}, respectively; Figure 4d and e). R_{Zn} values were low and relatively stable close to the primordium (1.1–6.1 μmol mol^{-1}), while rising monotonically in average and variability towards the otolith edge (4.4–25.6 μmol mol^{-1}, Figure 4f). R_{Sr} and R_{Ba}, on the other hand, exhibited a pattern of initially declining values to a minimum at approximately 100 dph (2.1–2.5 mmol mol^{-1} and 0.3–0.9 μmol mol^{-1}, respectively), followed by rising R until the edge (2.3–3.5 mmol mol^{-1} and 1.1–2.2 μmol mol^{-1}, respectively; Figure 4g and h).

When expressed relative to the day before catch (dpc), all R_E's except R_{Mn} showed a substantial increase in average values ($n = 24$, fitted with a non-parametric LOESS smoother) starting at ~60 dpc (Figure 5a–h). This increase was especially notable for R_{Ba} (1.3 → 1.8 μmol mol^{-1}), R_{Mg} (150 → 290 μmol mol^{-1}), R_{Co} (0.3 → 1.5 μmol mol^{-1}), and R_{Cu} (0.1 → 5.0 μmol mol^{-1}), while remaining weak or ambiguous for R_{Sr}, R_{Zn}, and R_{Li}. We interpreted this "edge signal" as potentially related to the entry of PBT juveniles into the CCLME and thus examined it further for each individual separately. For these analyses, we first standardized each replicate R_E value (i) for Ba, Mg, Co, and Cu to unit mean (mR_E) and standard deviation (sdR_E) for each element (j) and individual (k)

$$ZR_{E(i,j,k)} = \frac{R_{E(i,j,k)} - mR_{E(j,k)}}{sdR_{E(j,k)}},$$

and then combined the standardized ratios (ZR_E) to plot them against the date of deposition for each individual (Figure 6). Mean ZR_E's, calculated for each individual across all replicate values per ablation row, revealed a visually detectable increase ("edge signal") in 16 of 24 individuals, with statistical significance in 10 individuals (two-tailed t-test with unequal variances, comparing mean ZR_E's of each otoliths last ablation row with the values of the three preceding rows, d.f. = 14, $p < 0.05$, Figure 6). The remaining individuals showed neither increasing nor decreasing ZR_E values towards the otolith edge. Given the strong correlation between R_{Ba}, R_{Mg}, R_{Co}, and R_{Cu} within the four terminal ablation rows (~150 dpc, Pearson correlation coefficient 0.18–0.6, $p < 0.001$), a comparable pattern emerged, when analyses were conducted separately for each of the four elements (supplementary material, Figures S1–S4). We found that the difference in R_E's between the last and the three preceding ablation rows was unrelated to fish size (CFL), age, hatch, or sampling date (Pearson correlation, $p > 0.05$), but showed a tendency to increase with decreasing distance between the otolith edge and the last ablation row (Pearson correlation; Ba: $p = 0.057$, Mg: $p = 0.033$). Hence, the closer our ablations were performed to the otolith edge, the more likely we detected an increase in R_E. If the "edge signal" is in fact related to PBT moving from open ocean waters into the CCLME, our reconstruction revealed a likely entry window between late June and early August in 2012. However, a few individuals also showed conspicuous ZR_E increases as early as March/April 2012 (Figure 6).

Discussion

This study combined otolith microstructure and trace element analyses in juvenile PBT using a digital overlay approach to allow associating age estimates with individual ablation spots. This facilitated an age-resolved longitudinal examination of elemental patterns and a first test of whether the transition of juvenile tuna migrants from oligotrophic open Pacific Ocean into CCLME waters could be detected in their otoliths. Indeed, more than half of the examined individuals showed significant increases in Ba, Mg, Co, and Cu signatures at their otolith edge, which is consistent with such an "entry signal". An increase in Ba is consistent with exposure to upwelled water from depth (Lea *et al.*, 1989; Patterson *et al.*, 2004; Elsdon *et al.*, 2008; McMahon *et al.*, 2013), because Ba is enriched in deeper compared with surface waters. Recently, Woodson *et al.* (2013) showed that patchy upwelling in the CCLME can locally elevate Ba:Ca ratios in seawater from 5.5 to >6.5 μmol mol^{-1}, and that this signal was detectable in the otoliths of juvenile rockfish, where otolith Ba:Ca ratios increased correspondingly from ~0.5 to ~1.8 μmol mol^{-1}. Hence, the study showed that while absolute Ba concentrations in fish otoliths might be lower compared with seawater, changes in Ba exposure are likely translated into different otolith signatures (Woodson

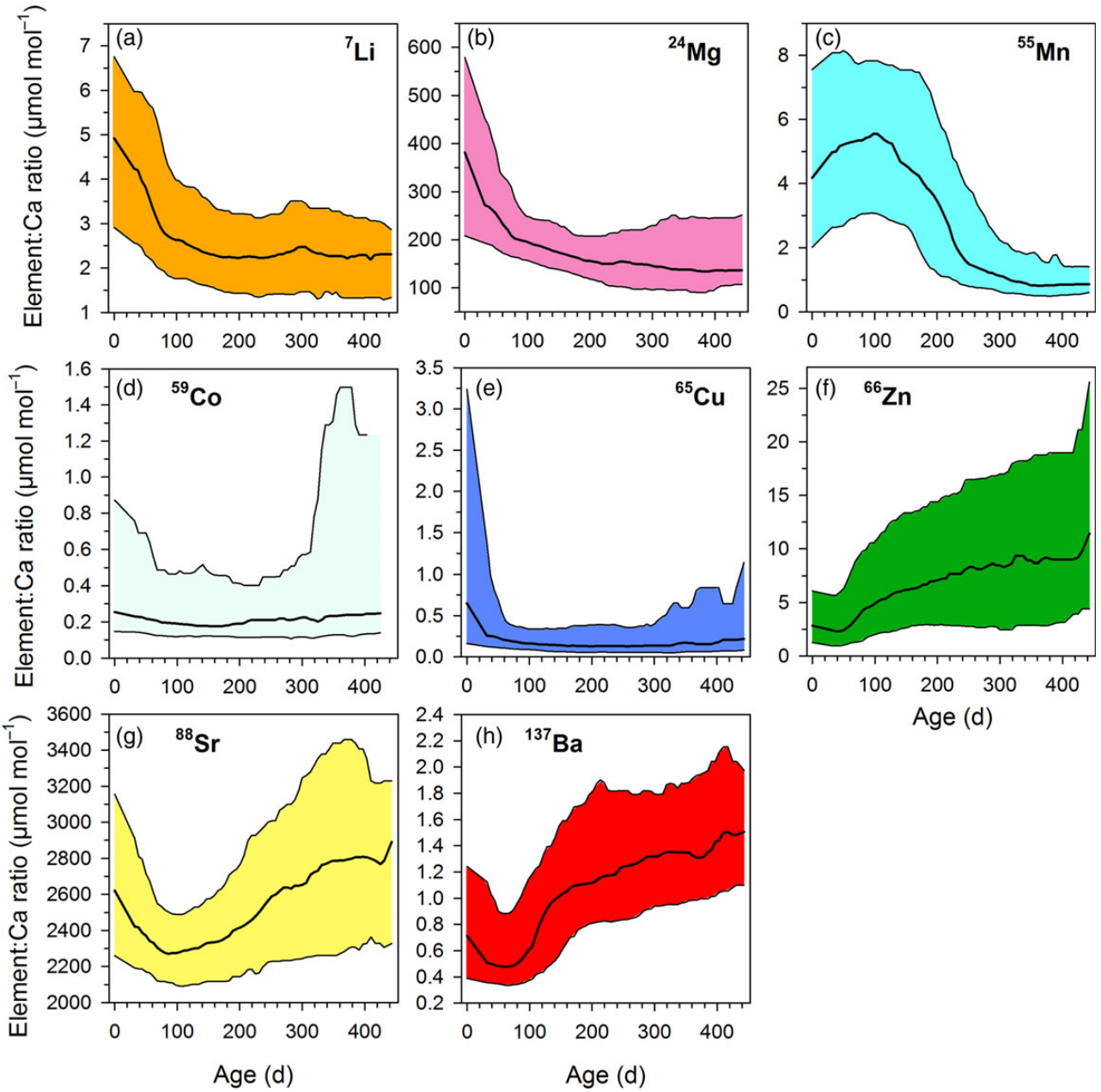

Figure 4. Average ontogenetic patterns in Element:Ca ratios (R_E) for (a) Li, (b) Mg, (c) Mn, (d) Co, (e) Cu, (f) Zn, (g) Sr, and (h) Ba of PBT juveniles caught in the CCLME in 2012. Shapes (10–90th percentiles) and thick black lines (median) were derived from age-dependent cumulative probability distributions of all replicate R_E's calculated using locally weighted, non-parametric density estimators with variable bandwidths. The non-parametric method is described in detail, for example, in Pepin *et al.* (1999) or Evans (2000). This figure is available in black and white in print and in colour at *ICES Journal of Marine Science* online.

et al., 2013). Our study found similar Ba:Ca ratios in juvenile PBT otoliths, with values <1 µmol mol^{-1} during most of the longitudinal record, but rapid increases at the otolith edge from a mean (s.d.) of 1.3 (0.3) to 1.8 (0.8) µmol mol^{-1} (Supplementary material, Figure S1).

In addition to Ba, conspicuous increases at the otolith edge were also detected for two trace metals, Co and Cu. Both elements are known to occur at very low concentrations in surface waters of the open North Pacific Ocean (Cu: 0.5 nmol kg^{-1}, Bruland, 1980), which is consistent with concentrations below detection limit along almost the entire longitudinal section of each otolith. Sediments from the Californian shelf, however, have been identified as significant external sources of Co and Cu (Bruland, 1980; Biller and Bruland, 2013), which may plausibly enrich the shelf waters of the CCLME (e.g. Cu: ~1.5 nmol kg^{-1}). This is consistent with the observed large Cu and Co increases at the otolith edge of some PBT juveniles. The concomitant increase in Mg in many specimens, on the other hand, might be incidental or comprise a by-product of migrants feeding on different prey while transitioning from the outside to the inside of the CCLME (Madigan *et al.*, 2014). Of the remaining four elements, three (Li, Zn, Sr) showed gradual instead of sudden increases towards the otolith edge, perhaps

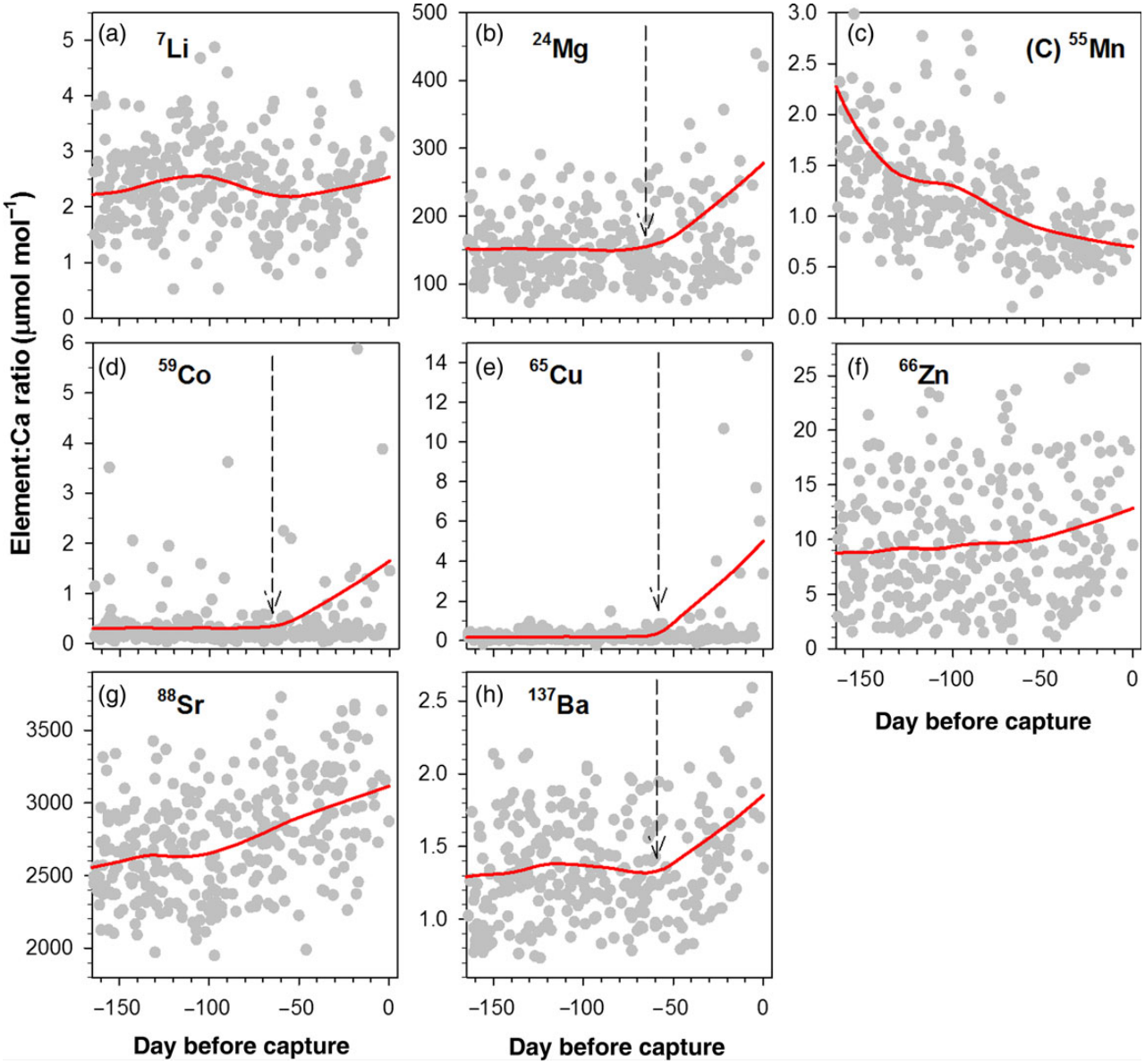

Figure 5. Element:Ca ratios (R_E) for Li (a), Mg (b), Mn (c), Co (d), Cu (e), Zn (f), Sr (g), and Ba (h) during the last 5 months before capture (160 dpc) of PBT juveniles in the CCLME. Grey dots depict each replicate R_E of all 24 individuals, which were fitted with a non-parametric Loess smoother (red line) with a bandwidth equal to 20% of data. Dashed arrows in b, d, e, and h indicate the observed increase in R_E at ~60 dpc. This figure is available in black and white in print and in colour at *ICES Journal of Marine Science* online.

reflecting an increase in seawater concentrations combined with a high degree of physiological modulation. Manganese, however, consistently decreased from primordium to edge in PBT otoliths, despite the scarcity of this element in surface waters of the open North Pacific central gyre (0.6–1.0 nmol kg^{-1}) compared with the coastal boundary of the CCLME (2–6 nmol kg^{-1}, Landing and Bruland, 1980).

While more than half of all individuals showed increasing R_{Ba}, R_{Mg}, R_{Cu}, and R_{Co} at the otolith edge, a considerable fraction lacked this "entry signal", despite being landed inside the CCLME. Some individuals might have simply arrived too recently before catch and thus did not deposit sufficient otolith material for inclusion in our terminal ablation spots. This is supported by the fact that recreational catches of the new, age-1 PBT cohort still increase in proportion through August, i.e. close to the sampling dates of this study (Figure 7; and discussed below). Furthermore, the placement of terminal ablation spots was dictated by a practical trade-off between ablating close to the otolith edge while avoiding artefacts due to splintering or partial ablations. In a few cases, this likely led to greater-than-desired edge distances, which reduced the probability of detecting the entry signal. Another possible reason for our results is the spatio-temporal heterogeneity of the CCLME itself, where seasonal upwelling occurs in patchy and ephemeral episodes, depending on the changes in windstress, bottom bathymetry, and coastline structure (Mann and Lazier, 2006). Hence, even for PBT juveniles inside the CCLME, the elemental signal related to upwelling would be expected to vary substantially depending on the water masses the fish actually encountered (Woodson *et al.*, 2013). While

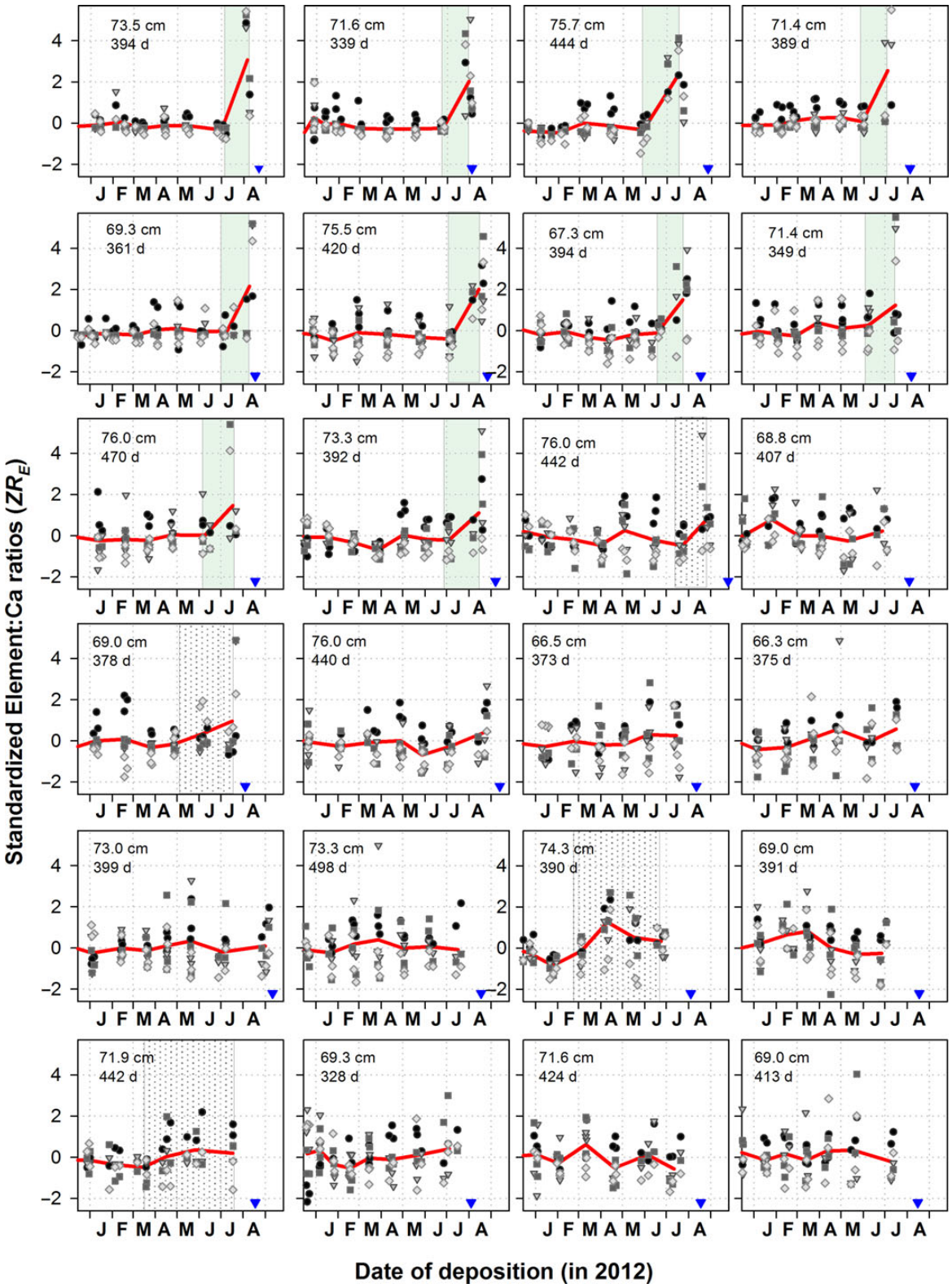

Figure 6. Standardized Element:Ca ratios (ZR_E) of Mg (diamonds), Co (triangles), Cu (squares), and Ba (circles) for all 24 individual PBT juveniles used in this study. Points represent individual ablation spots plotted against the estimated date of deposition. Red lines connect means, calculated by averaging all ZR_E's per ablation row. Blue triangles denote the catch date; CFL (cm) and total age estimates (d) are given for each individual. Green shaded panels correspond to individuals, which had significantly higher ZR_E's in the last ablation row compared to the preceding three ablation rows. Some other individuals showed either subtle or unexpectedly early increases in mean ZR_E's, potentially indicating an earlier entrance into the CCLME.

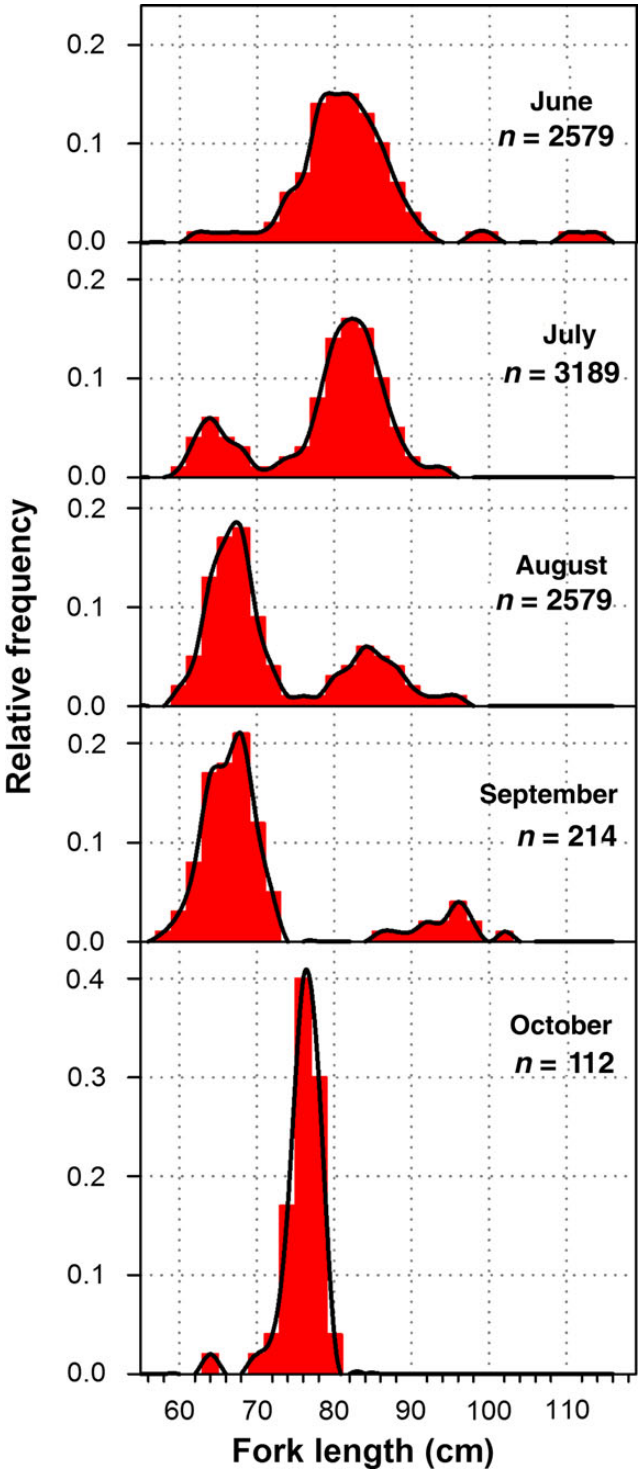

Figure 7. Relative length frequency distributions of monthly recreational PBT catches off the coast of San Diego, CA (Data: Southwest Fisheries Science Center, NOAA, 2005–2012). This figure is available in black and white in print and in colour at *ICES Journal of Marine Science* online.

following their prey, tunas move both horizontally and vertically through waters that likely possess different elemental signatures, thereby blurring the geochemical signal of any one in particular (Kitagawa *et al.*, 2007). Although the approach shows considerable promise, the absence of an entry signal in some individuals suggests that additional research is needed to assess the reliability of these natural markers and the required length of residency in the CCLME for PBT to acquire the entry signal.

For specimens that exhibited a signal consistent with entry into the CCLME, the reconstructed window of arrival generally occurred between late June and early August 2012. This entry period is consistent with Madigan *et al.* (2014), who combined three biochemical tracer approaches and deduced that the majority of age 1–2 PBT arrive in the Eastern Pacific Ocean between May and August. It is also in good agreement with the long-term seasonal pattern of recreational PBT catches off Southern California as recorded by the Inter American Tropical Tuna Commission (IATTC) and NOAA SWFSC. Average monthly length frequency distributions (June–October) of PBT caught between 2005 and 2012 ($n = 8673$) clearly show that a new cohort of individuals (60–70 cm FL) first appears gradually from June to July and then increasingly dominates the catches in August–September (Figure 7). Despite the known limitations of recreational fishery data (e.g. seasonally varying effort, boat size, trip length, angler experience, temperature-dependent tuna catchability), the general pattern strongly corroborates our estimated window of arrival for new PBT migrants between late June and August, highlighting the potential value of using otoliths to estimate the timing of migrations.

Recently, Madigan *et al.* (2012, 2013, 2014) measured concentrations of anthropogenic radiocesium (i.e. ^{134}Cs and ^{137}Cs, released from the failed Fukushima nuclear power plant in 2011; Buesseler *et al.*, 2012) in muscle tissue of similarly collected PBT juveniles. Using estimates of efflux and the differential decay rates of the two isotopes, the study modelled how tissue ^{134}Cs:^{137}Cs ratios would decrease once fish had left Japanese waters, which in turn allowed reconstructing their time of departure. Estimates ranged from 30 to 80 d since departure (mean = 50 d) and translated into a general departure window centered in early June 2012 (range: mid-May to early July). When combined, the estimated departure (Madigan *et al.*, 2013) and arrival windows (this study) suggest that juvenile PBT migrants require ~1.5–2 months to complete their trans-Pacific migration (a distance of ~8000 km; Orange and Fink, 1963). This estimate is consistent with the single available observation of a PBT juvenile that was archival tagged in November 1996 in the East China Sea and crossed the North Pacific Ocean 1 year later, in 64 d (Itoh *et al.*, 2003; Kitagawa *et al.*, 2009). In this case, however, the trans-Pacific migration occurred during winter (December–January; consistent with older migrants: Madigan *et al.*, 2014), not at the end of spring as inferred for the age-1 individuals of this study. While conventional tags have also shown west–east migrations (Bayliff *et al.*, 1991; Bayliff, 1994), the lack of information on location between tag and release makes it impossible to accurately determine the timing.

Otolith microstructure analysis of PBT juveniles added valuable information and ontogenetic context to otolith chemical measurements, despite the increased ageing uncertainty in such relatively old fish. Sagittal otoliths in tunas exhibit discernible, year-round, daily growth (at least through age-1) that in theory allows reconstructing several hundred days into the past (Wild and Foreman, 1980; Lehodey and Leroy, 1999), in contrast to many temperate fish species, where strong winter ring formation usually limits otolith microstructure analysis strictly to the young of the year. Interpreting the microstructure in juvenile PBT otoliths, however, can be challenging, because the innermost increments are often difficult to discern (e.g. caused by a slight offset of the polished

transversal section from the actual primordium) and areas of poor increment visibility may require variable measurement paths. Additional uncertainty was inherent to our digital overlay method, which constructed age contour grids to extrapolate the otolith microstructure beyond the immediate areas of observation. Despite these challenges, blind within-reader ageing precision was sufficiently high (CV = 5.7%), and the corresponding hatch distribution (i.e. April to September, with the majority born in June, July, and August; Figure 3b) was highly consistent with published data and general knowledge about PBT spawning in the western Pacific Ocean. For example, Tanaka *et al.* (2007) applied otolith microstructure analysis to PBT juveniles (10–28 cm) collected in 1999 and 2004 in the Sea of Japan, reporting inferred ages of 43–93 dph and corresponding hatch dates mainly in July and to some extent in June. Our data are also consistent with Chen *et al.* (2006) and Kitagawa *et al.* (1995) who showed that the spawning season of PBT in the East China Sea usually extends from May to July, but occurs later during July and August in the Sea of Japan. This temporal shift in spawning times between two principal PBT spawning grounds has been widely documented in the literature (Yabe *et al.*, 1966; Okiyama, 1974; Suzuki *et al.*, 2014), and our back-calculated hatch dates encompassed the spawning seasons of both spawning grounds. In contrast, age back-calculations based on age–length relationships such as those in Bayliff *et al.* (1991) and Shimose *et al.* (2009) (e.g. used in Madigan *et al.*, 2013) appear to overestimate the age of immigrating PBT juveniles; when we used these relationships on our current specimens the hatch-date distribution would have shifted unrealistically into the months of February and March (Supplementary material, Figure S5).

In summary, longitudinal microchemistry in fish otoliths offers a wealth of informative, high-resolution data that can be complemented by otolith microstructure analysis. Here, the approach revealed that the otoliths of juvenile PBT (US West Coast) likely contain a trace elemental signal that coincides with the entry of these fish into the CCLME after their ~8000 km trans-Pacific journey. Several elements (Ba, Mg, Co, Cu) appeared useful to identify a CCLME signal, but the validity of this signal will depend on a more robust characterization of spatio-temporal element patterns from seawater samples in and outside of the CCLME. Future work should also include outside groups or controls such as older CCLME residents (e.g. ages 3–5), or fish that have been in a known location (e.g. tuna farms), or fish from which archival tags are recovered and retrospective migratory patterns are known. Further work is also required to refine ablation and image analysis techniques, and increase sample sizes. Ultimately, the method may have the potential to inform managers deciding the timing and catch limits of PBT fisheries and thus help improve the overfished state of the PBT stock.

Supplementary data

Supplementary material is available at the *ICESJMS* online version of the manuscript.

Acknowledgments

We are grateful to the many recreational fishers, captains, and crews for donating fish carcasses, to the IATTC and the Sportfishing Association of California for helping to facilitate the sampling programme, and to Fisherman's Processing for allowing sample collections. Student volunteers at the Southwest Fisheries Science Center helped processing fish heads and cleaning otoliths.

Funding

This study was funded by Grant No. 3423 from the Gordon and Betty Moore Foundation and partially by the National Science Foundation Postdoctoral Research Fellowship in Biology under Grant No. 1305791 (to D.J.M.).

References

Baumann, H., Hinrichsen, H. H., Voss, R., Stepputtis, D., Grygiel, W., Clausen, L. W., and Temming, A. 2006. Linking growth to environmental histories in central Baltic young-of-the-year sprat, *Sprattus sprattus*: an approach based on otolith microstructure analysis and hydrodynamic modelling. Fisheries Oceanography, 15: 465–476.

Bayliff, W. H. 1994. A review of the biology and fisheries for northern bluefin tuna, *Thunnus thynnus*, in the Pacific Ocean. FAO Fisheries Technical Paper 336/2:244–295 (FAO).

Bayliff, W. H., Ishizuki, Y., and Deriso, R. B. 1991. Growth, movement, and attrition of northern bluefin tuna, Thunnus thynnus, in the Pacific Ocean, as determined by tagging. Inter-American Tropical Tuna Commission Bulletin, 20: 1–94.

Biller, D. V., and Bruland, K. W. 2013. Sources and distributions of Mn, Fe, Co, Ni, Cu, Zn, and Cd relative to macronutrients along the central California coast during the spring and summer upwelling season. Marine Chemistry, 155: 50–70.

Block, B. A., Jonsen, I., Jorgensen, S., Winship, A., Shaffer, S. A., Bograd, S., Hazen, E., *et al.* 2011. Tracking apex marine predator movements in a dynamic ocean. Nature, 475: 86–90.

Boustany, A. M., Matteson, R., Castleton, M., Farwell, C., and Block, B. A. 2010. Movements of Pacific bluefin tuna (*Thunnus orientalis*) in the Eastern North Pacific revealed with archival tags. Progress in Oceanography, 86: 94–104.

Bruland, K. W. 1980. Oceanographic distributions of cadmium, zinc, nickel, and copper in the North Pacific. Earth and Planetary Science Letters, 47: 176–198.

Buesseler, K. O., Jayne, S. R., Fisher, N. S., Rypina, I. I., Baumann, H., Baumann, Z., Breier, C. F., *et al.* 2012. Fukushima-derived radionuclides in the ocean and biota off Japan. Proceedings of the National Academy of Sciences of the United States of America, 109: 5984–5988.

Campana, S. E. 2001. Accuracy, precision and quality control in age determination, including a review of the use and abuse of age validation methods. Journal of Fish Biology, 59: 197–242.

Campana, S. E. 2005. Otolith science entering the 21st century. Marine and Freshwater Research, 56: 485–495.

Campana, S. E., Chouinard, G. A., Hanson, J. M., Fréchet, A., and Brattey, J. 2000. Otolith elemental fingerprints as biological tracers of fish stocks. Fisheries Research, 46: 343–357.

Campana, S. E., and Thorrold, S. R. 2001. Otoliths, increments, and elements: keys to a comprehensive understanding of fish populations? Canadian Journal of Fisheries and Aquatic Sciences, 58: 30–38.

Chen, K-S., Crone, P., and Hsu, C-C. 2006. Reproductive biology of female Pacific bluefin tuna T*hunnus orientalis* from south-western North Pacific Ocean. Fisheries Science, 72: 985–994.

Collette, B., Carpenter, K., Polidoro, B., Juan-Jordá, M., Boustany, A., Die, D., Elfes, C., *et al.* 2011. High value and long life-double jeopardy for tunas and billfishes. Science, 333: 291–292.

Collette, B. B., and Nauen, C. E. 1983. FAO species catalogue. Vol 2: Scombrids of the world. FAO Fishery Synopsis, 125: 122–136.

Elsdon, T. S., Wells, B. K., Campana, S. E., Gillanders, B. M., Jones, C. M., Limburg, K. E., Secor, D. H., *et al.* 2008. Otolith chemistry to describe movements and life-history parameters of fishes: hypotheses, assumptions, limitations and inferences. Oceanography and Marine Biology: an Annual Review, 46: 297–330.

Evans, G. T. 2000. Local estimation of probability distribution and how it depends on covariates. Canadian Stock Assessment Secretariat Research Document, 120: 11.

ISC. 2014. Pacific bluefin stock assessment. International Scientific Committee for Tuna and Tuna-like Species in the North Pacific Ocean, Shimizu, Shizuoka, Japan.

Itoh, T., Shiina, Y., Tsuji, S., Endo, F., and Tezuka, N. 2000. Otolith daily increment formation in laboratory reared larval and juvenile bluefin tuna *Thunnus thynnus*. Fisheries Science, 66: 834–839.

Itoh, T., Tsuji, S., and Nitta, A. 2003. Migration patterns of young Pacific bluefin tuna (*Thunnus orientalis*) determined with archival tags. Fishery Bulletin, 101: 514–534.

Kerr, L. A., Secor, D. H., and Piccoli, P. M. 2009. Partial migration of fishes as exemplified by the estuarine-dependent white perch. Fisheries, 34: 114–123.

Kitagawa, T., Boustany, A. M., Farwell, C. J., Williams, T. D., Castleton, M. R., and Block, B. A. 2007. Horizontal and vertical movements of juvenile bluefin tuna (*Thunnus orientalis*) in relation to seasons and oceanographic conditions in the eastern Pacific Ocean. Fisheries Oceanography, 16: 409–421.

Kitagawa, T., Kimura, S., Nakata, H., Yamada, H., Nitta, A., Sasai, Y., and Sasaki, H. 2009. Immature Pacific bluefin tuna, *Thunnus orientalis*, utilizes cold waters in the Subarctic Frontal Zone for trans-Pacific migration. Environmental Biology of Fishes, 84: 193–196.

Kitagawa, Y., Nishikawa, Y., Kubota, T., and Okiyama, M. 1995. Distribution of ichthyoplanktons in the Japan Sea during summer, 1984, with special reference to scombroid fishes. Bulletin of the Japanese Society of Fisheries Oceanography (Japan), 59: 107–114.

Landing, W. M., and Bruland, K. W. 1980. Manganese in the North Pacific. Earth and Planetary Science Letters, 49: 45–56.

Lea, D. W., Shen, G. T., and Boyle, E. A. 1989. Coralline barium records temporal variability in equatorial Pacific upwelling. Nature, 340: 373–376.

Lehodey, P., and Leroy, B. 1999. Age and growth of yellowfin tuna (*Thunnus albacares*) from the western and central Pacific Ocean as indicated by daily growth increments and tagging data. WP YFT-2, SCTB, 12: 16–23.

Madigan, D. J., Baumann, Z., Carlisle, A. B., Hoen, D. K., Popp, B. N., Dewar, H., Snodgrass, O. E., *et al.* 2014. Reconstructing transoceanic migration patterns of Pacific bluefin tuna using a chemical tracer toolbox. Ecology, 95: 1674–1683.

Madigan, D. J., Baumann, Z., and Fisher, N. S. 2012. Pacific bluefin tuna transport Fukushima-derived radionuclides from Japan to California. Proceedings of the National Academy of Sciences of the United States of America, 109: 9483–9486.

Madigan, D. J., Baumann, Z., Snodgrass, O. E., Ergül, H. A., Dewar, H., and Fisher, N. S. 2013. Radiocesium in Pacific Bluefin Tuna *Thunnus orientalis* in 2012 validates new tracer technique. Environmental Science & Technology, 47: 2287–2294.

Mann, K., and Lazier, J. 2006. Dynamics of Marine Ecosystems: Biological-Physical Interactions in the Oceans. 3rd edn. Blackwell Publishing Malden, MA, USA. ISBN-13: 978-1-4051-1118-8.

McMahon, K. W., Hamady, L. L., and Thorrold, S. R. 2013. A review of ecogeochemistry approaches to estimating movements of marine animals. Limnology and Oceanography, 58: 697–714.

Morrongiello, J. R., Thresher, R. E., and Smith, D. C. 2012. Aquatic biochronologies and climate change. Nature Climate Change, 2: 849–857.

Okiyama, M. 1974. Occurrence of the postlarvae of bluefin tuna, *Thunnus thynnus*, in the Japan Sea. Bulletin of the Japan Sea Regional Fisheries Research Laboratory, 25: 89–97.

Orange, C. J., and Fink, B. D. 1963. Migration of a tagged bluefin tuna across the Pacific Ocean. California Fish and Game, 49: 307–308.

Patterson, H. M., Kingsford, M. J., and McCulloch, M. T. 2004. The influence of oceanic and lagoonal plume waters on otolith chemistry. Canadian Journal of Fisheries and Aquatic Sciences, 61: 898–904.

Pepin, P., Evans, G. T., and Shears, T. H. 1999. Patterns of RNA/DNA ratios in larval fish and their relationship to survival in the field. ICES Journal of Marine Science, 56: 697–706.

Rooker, J. R., Alvarado Bremer, J. R., Block, B. A., Dewar, H., de Metrio, G., Corriero, A., Kraus, R. T., *et al.* 2007. Life history and stock structure of Atlantic bluefin tuna (*Thunnus thynnus*). Reviews in Fisheries Science, 15: 265–310.

Rooker, J. R., Secor, D. H., De Metrio, G., Schloesser, R., Block, B. A., and Neilson, J. D. 2008. Natal homing and connectivity in Atlantic bluefin tuna populations. Science, 322: 742–744.

Rooker, J. R., Secor, D. H., Zdanowicz, V. S., and Itoh, T. 2001b. Discrimination of northern bluefin tuna from nursery areas in the Pacific Ocean using otolith chemistry. Marine Ecology Progress Series, 218: 275–282.

Rooker, J. R., Zdanowicz, V., and Secor, D. 2001a. Chemistry of tuna otoliths: assessment of base composition and postmortem handling effects. Marine Biology, 139: 35–43.

Shimose, T., Tanabe, T., Chen, K-S., and Hsu, C-C. 2009. Age determination and growth of Pacific bluefin tuna, *Thunnus orientalis*, off Japan and Taiwan. Fisheries Research, 100: 134–139.

Stevenson, D. K., and Campana, S. E. 1992. Otolith microstructure examination and analysis. Canadian Special Publication in Fisheries and Aquatic Sciences 117. Department of Fisheries and Oceans, Ottawa, Canada. 126 pp.

Suzuki, N., Tanabe, T., NOhara, K., Doi, W., Ashida, H., Kameda, T., and Aonuma, Y. 2014. Annual fluctuation in Pacific bluefin tuna (*Thunnus orientalis*) larval catch from 2007 to 2010 in waters surrounding the Ryukyu Archipelago, Japan. Bulletin of the Fisheries Research Agency, 38: 87–99.

Tanaka, Y., Mohri, M., and Yamada, H. 2007. Distribution, growth and hatch date of juvenile Pacific bluefin tuna *Thunnus orientalis* in the coastal area of the Sea of Japan. Fisheries Science, 73: 534–542.

Thorrold, S. R., Campana, S. E., Jones, C. M., and Swart, P. K. 1997. Factors determining δ13C and δ18O fractionation in aragonitic otoliths of marine fish. Geochimica et Cosmochimica Acta, 61: 2909–2919.

Veinott, G., and Porter, R. 2005. Using otolith microchemistry to distinguish Atlantic salmon (*Salmo salar*) parr from different natal streams. Fisheries Research, 71: 349–355.

Wild, A., and Foreman, T. 1980. The relationship between otolith increments and time for yellowfin and skipjack tuna marked with tetracycline. Inter-American Tropical Tuna Commission Bulletin, 17: 507–560.

Woodson, L., Wells, B., Grimes, C., Franks, R., Santora, J., and Carr, M. 2013. Water and otolith chemistry identify exposure of juvenile rockfish to upwelled waters in an open coastal system. Marine Ecology Progress Series, 473: 261–273.

Yabe, H., Ueyanagi, S., and Watanabe, H. 1966. Studies on the early life history of bluefin tuna *Thunnus thynnus* and on the larvae of the southern bluefin tuna *T. maccoyii*. Reports of the Nankai Regional Fisheries Research Lab, 23: 95–129.

Handling editor: Dr David Secor